Journal of Natural Disaster Science, Volume 16, *Number* 2, 1995, *pp.* 1–22

PREDICTION OF PROBABLE SURFACE FAILURE USING 3-D SLOPE STABILITY ANALYSES AND THE SLIDING DIRECTION

Takashi OKIMURA
(Associate Professor, Reclamation Engineering Research Institute, Faculty of Engineering, Kobe University, Nada Kobe 657, Japan)

(Received 23 March, 1994 and in revised form 8 February, 1995)

ABSTRACT

A three-dimensional slope stability analysis method, called the three-dimensional multi-planar sliding surface method, was proposed previously (Okimura & Maeda [5]; Okimura & Morimoto [6]). It gives the site and volume of the critical sliding mass, as defined by the minimum safety factor. The method for shaping an assumed sliding mass that is nonrectangular in plan has been defined by taking into account the equilibrium of the forces between columns within an assumed sliding mass (Okimura [7]). In these studies, the sliding direction of the assumed sliding mass was set parallel to the steepest direction of the most unstable cell that had been found as proposed previously (Okimura & Ichikawa [4]). The sliding direction of the assumed sliding mass, however, may change according to the shape of the assumed mass. A method for calculating the sliding direction is proposed that is based on the equilibrium of the forces being at a right angle to the sliding direction. It was applied to an actual mountain slope on which shallow failures caused by heavy rainfall had taken place. The sliding direction calculated by this method was nearly the same as that of the actual failed mass. Using the obtained sliding direction, the coordinates of a digital land elevation model were transformed and slope stability analyses made by three 3-D methods: the multi-planar sliding surface method, and the 3-D Hovland and the simplified Janbu methods. Results showed that the most critical sliding masses obtained using the calculated sliding direction were closer to the actual sliding masses than those obtained using the most unstable cell's sliding direction.

1. INTRODUCTION

Many methods for predicting the time of appearance of probable failure, of frequent occurrence on mountain slopes during heavy rainfall, have been proposed that are based on empirically obtained relations between actual failures and the time of the maximum rainfall intensity and/or the rainfall pattern [1], as well as on soil water calculations made analytically by means of the saturated and unsaturated seepage models [2]. Methods for predicting the probable failure site of an unstable mass also have been presented. Such models are meant to predict the site and length of the probable failure on a longitudinal section [3] and to predict the most probable unstable cell in a digital land elevation model [4]. Only a few paper, however, have reported prediction methods for probable unstable soil volume caused by shallow failure because the three-dimensional analyses used to predict probable failure on a mountain slope have yet to be fully developed.

To solve this problem, Okimura et al. [5] proposed a 3-D prediction method named the multi-planar sliding surface method (called the MPSS method, hereafter) which was developed from the 2-D method [3] for a cross sectional as well as a longitudinal plane. Okimura et al. [6], used the proposed 3-D prediction method and showed that the site of the most unstable mass was nearly the same as that of the failed mass and that the unstable volume calculated was nearly equal to the volume of the failed mass even though a different mesh space for the digital land

KEY WORDS: Prediction of mountain slope failure, Shallow failure, Three-dimensional slope stability analysis, Probable sliding direction, Digital elevation model

elevation model was used in the 3-D prediction method. A setting up method, giving an assumed sliding soil mass that is non-rectangular in plan shape, also was proposed for the 3-D prediction method on the basis of the continuity of the forces acting on an imaginary vertical wall between prismatic column elements (hereafter, called "columns") in the assumed sliding mass [7]. This method was applied to actual failed slopes, the safety factor being calculated using the 3-D MPSS, the 3-D Hovland [8], and 3-D simplified Janbu [9] methods. The results obtained were discussed in terms of the reliability of the prediction of the site and shape of the probable failure [7].

In these studies [5, 6 and 7], the sliding direction of the assumed sliding mass was set parallel to the steepest direction of the most unstable cell, determined as reported elsewhere [4]. The sliding direction of the assumed sliding mass, however, may change according to the shape of that mass. A method for calculating the sliding direction therefore is proposed that is based on the equilibrium of the force components being at a right angle to the sliding direction.

2. METHOD CALCULATING THE PROBABLE SLIDING DIRECTION

2.1 *Basis for the new method*

To predict the most probable critical sites using the methods described previously [5, 6 and 7], the most unstable cell (that part of a mountain slope enclosed by a grid space) first must be distinguished from the large catchment area by the method presented elsewhere [4]. The new method uses the digital elevation model, in which the potential failure layer [10] is defined, a cell being regarded as a column of the potential failure layer. In this new method, the digital elevation model is used in conjunction with a ground water movement model to calculate the height of the piezometric surface in the potential failure layer. The calculated piezometric height is then used in the infinite slope stability analysis. The safety factor of every cell is calculated hourly. The degree of instability of the column is defined by a continuous period that lasts until the safety factor decreases to less than unity because failure is considered to occur within a much shorter continuous period on a potentially unstable slope.

We identify the analysis area within the most critical sliding mass so as to include seven columns in the longitudinal and transverse directions, an area composed of 7×7 columns, the most unstable column appearing at the center. Many assumed sliding masses that are regarded to be rectangular in plan shape then are set up within this area so as to include the most unstable column. The sliding direction and safety factor of the assumed sliding mass is calculated by our new method as described hereafter. A sliding mass is assumed such that all combinations of columns are set, then the safety factor is obtained for each assumed sliding mass. The most critical sliding mass is regarded to be the one with the minimum safety factor value, its sliding direction being the answer given by the new method.

2.2 3-*D slope stability analysis for calculating the sliding direction*

A flowchart of the new method is given in Fig. 1. The method is hereafter on the basis of this explained flowchart.

(1) Equilibrium of the forces acting on a column

The forces acting on an imaginary vertical wall of a column were assumed to be the internal forces of the horizontal component, the vertical component of the internal forces caused by the shear force being ignored in this study. Fig. 2 shows the forces acting on a column. The symbols are defined as follows: $N_{i,j}$ is the normal force acting on the sliding surface, $Tm_{i,j}$ the mobilized resisting shear force acting on the sliding surface, $Hx_{i,j}$ the horizontal force in the X direction acting on an imaginary vertical wall, $Hy_{i,j}$ the horizontal force in the Y direction acting on an imaginary vertical wall, $W_{i,j}$ the weight of the column, $\alpha_{i,j}$ the inclination angle along the sliding

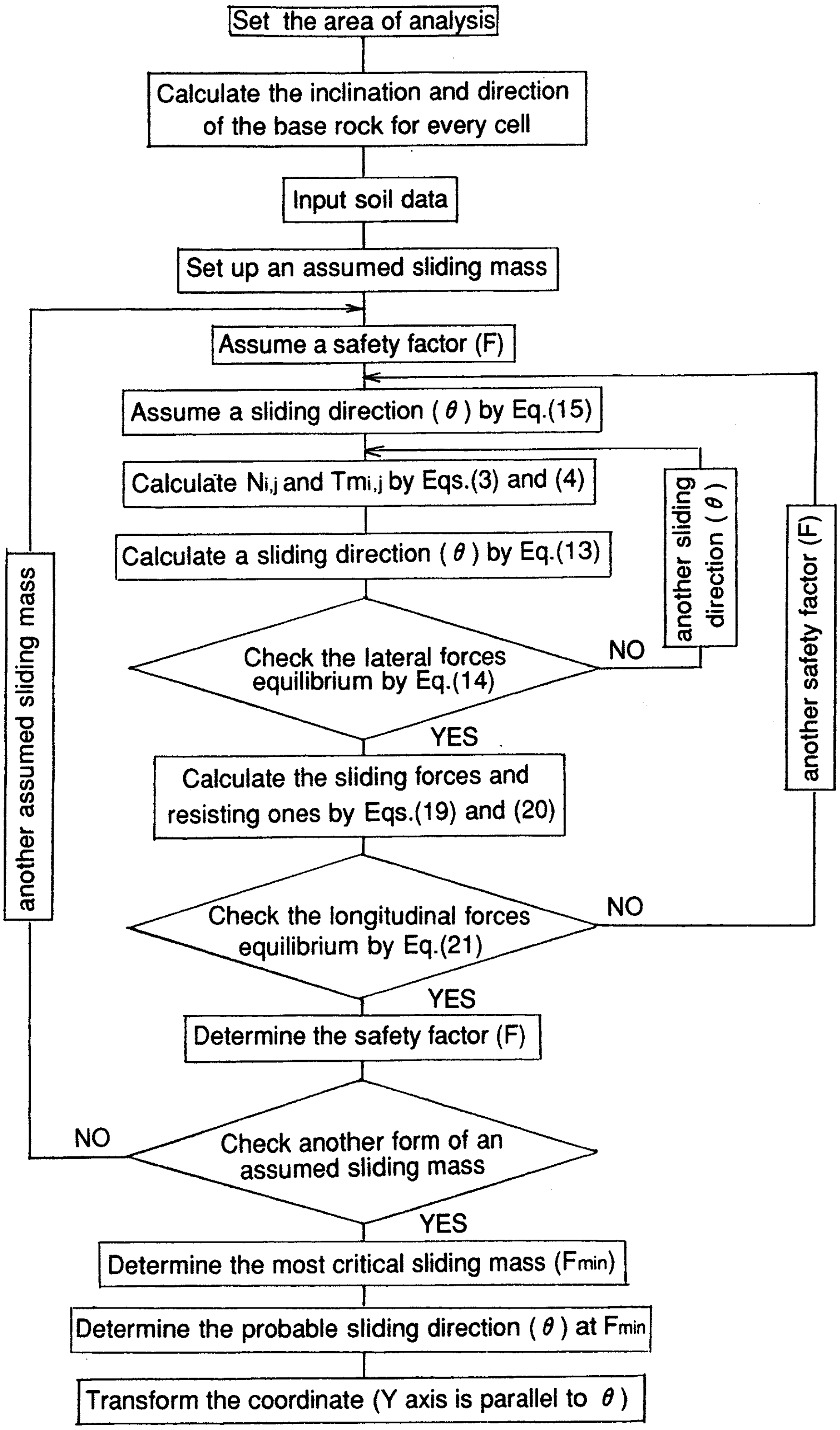

Fig. 1. Flowchart of the proposed method for calculating the sliding direction

direction, $\beta_{i,j}$ the steepest inclination of the column base, $\theta'_{i,j}$ the angle projected on the X-Y plane between the direction of the steepest inclination and the X axis, and θ the angle projected on the X-Y plane between the sliding direction and the X axis.

The following equation is based on the equilibrium of the vertical direction;

$$N_{i,j}\cdot\cos\beta_{i,j}+Tm_{i,j}\cdot\sin\alpha_{i,j}-W_{i,j}=0 \qquad (1)$$

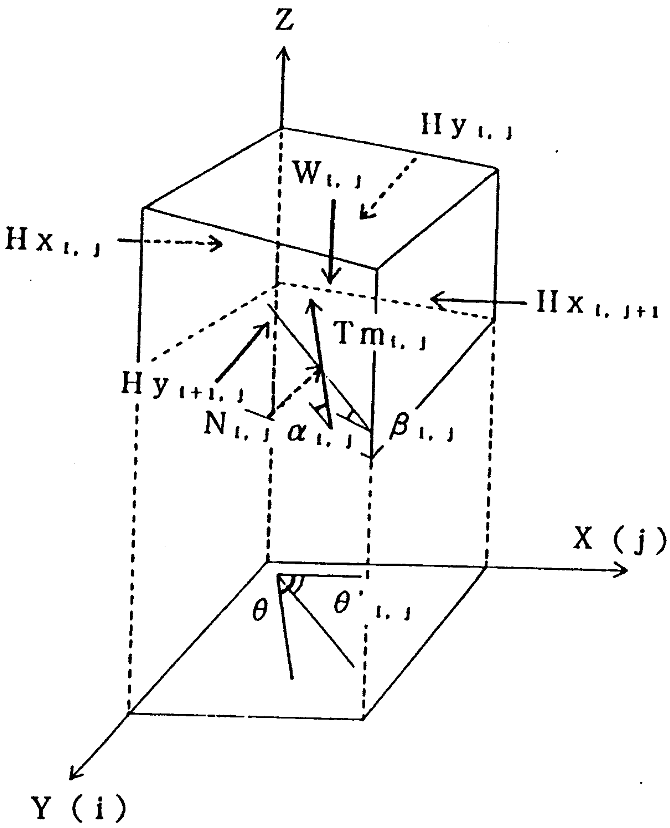

Fig. 2. Forces acting on a column (for the j-th column of the i-th line)

The shear strength of $T_{i,j}$ is obtained using the Mohr-Coulomb failure criterion.

$$T_{i,j}=c\cdot A_{i,j}+N_{i,j}\cdot\tan\phi \tag{2}$$

in which, c is the cohesion strength, ϕ the internal friction angle, and $A_{i,j}$ the area of the sliding surface.

The mobilized resisting shear force of $Tm_{i,j}$ is expressed by

$$Tm_{i,j}=\frac{T_{i,j}}{F}=\frac{c\cdot A_{i,j}+N_{i,j}\cdot\tan\phi}{F} \tag{3}$$

in which, F is the safety factor.

$N_{i,j}$ is presented by the following equation, the rearrangement obtained by substituting Eq. (3) in Eq. (1);

$$N_{i,j}=\frac{W_{i,j}-\dfrac{c\cdot A_{i,j}}{F}\sin\alpha_{i,j}}{\cos\beta_{i,j}+\dfrac{\tan\phi}{F}\sin\alpha_{i,j}} \tag{4}$$

The inclination of the resisting direction $\alpha_{i,j}$, is defined by the following equation (see Fig. 3);

$$\sin\alpha_{i,j}=\frac{\mathrm{w}\cdot\sin\theta+\mathrm{v}\cdot\cos\theta}{\sqrt{1+(\mathrm{w}\cdot\sin\theta+\mathrm{v}\cdot\cos\theta)^2}} \tag{5}$$

in which $1/\mathrm{v}$ is the intercept of the X axis and $1/\mathrm{w}$ that of the Y axis.

Unknown factors in Eq. (4) therefore number only two, F and $N_{i,j}$. The force of $N_{i,j}$ is obtained by assuming F.

The following equations are obtained using the equilibria along the X and Y directions of the columns.

For the direction of the X axis,

$$N_{i,j}\cdot\sin\beta_{i,j}\cdot\cos\theta'_{i,j}-Tm_{i,j}\cdot\cos\alpha_{i,j}\cdot\cos\theta=Hx_{i,j+1}-Hx_{i,j}=\Delta Hx_{i,j} \tag{6}$$

For the direction of the Y axis,

$$N_{i,j}\cdot\sin\beta_{i,j}\cdot\sin\theta'_{i,j}-Tm_{i,j}\cdot\cos\alpha_{i,j}\cdot\sin\theta=Hy_{i+1,j}-Hy_{i,j}=\Delta Hy_{i,j} \tag{7}$$

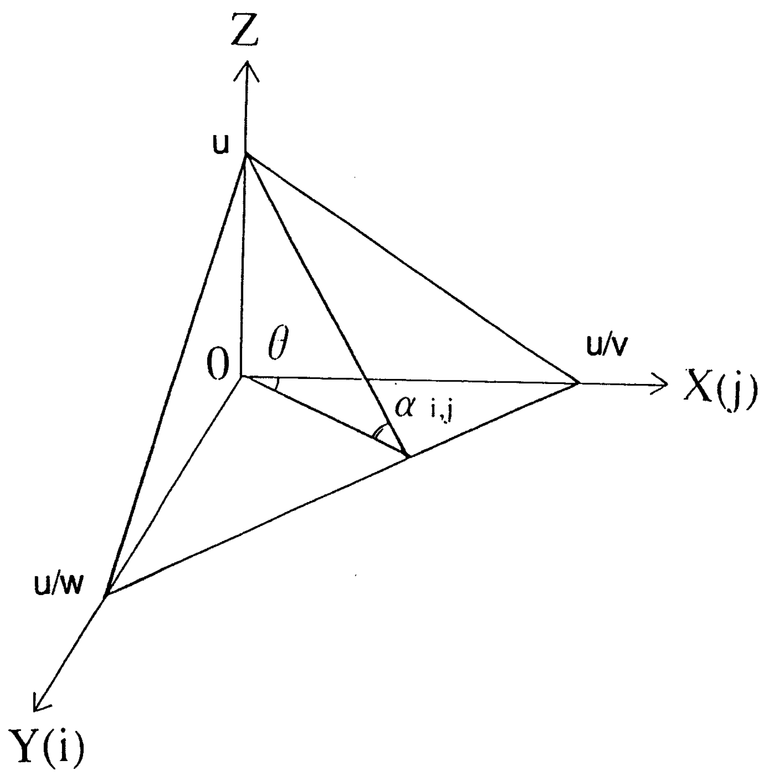

Fig. 3. Schematic diagram of the inclination of the sliding direction $\alpha_{i,j}$

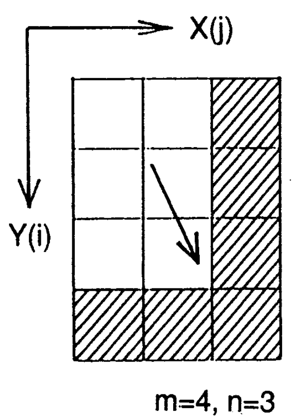

Fig. 4. Example of an assumed sliding mass composed of 4×3 columns. The arrow shows the sliding direction. The shaded columns show the lower end columns.

$\Delta Hx_{i,j}$ and $\Delta Hy_{i,j}$ in the above equations are the respective resultant forces acting on an imaginary vertical wall, in the X and the Y directions. Assuming F in Eqs. (6) and (7), the resultant forces of $\Delta Hx_{i,j}$ and $\Delta Hy_{i,j}$ are calculated by substituting $N_{i,j}$ (obtained by Eq. (4)) and $Tm_{i,j}$ (obtained by Eq. (3)) in these equations. The forces of $Hx_{i,j+1}$ and $Hy_{i+1,j}$ are obtained successively using Eqs. (6) and (7) by assuming the forces of $Hx_{i,1}$ and $Hy_{1,j}$ which act on the upper end wall of the assumed sliding mass.

(2) Calculation of the sliding direction

An assumed sliding mass rectangular in plan shape is set up using $m \times n$ columns in the longitudinal and transverse directions. Fig. 4 shows an example of an assumed sliding mass composed of 4×3 columns. The sliding direction for this example is assumed to be expressed by the arrow within the figure, the shaded columns being designated "the lower end columns" in this study. The force equilibrium in the X direction is expressed by the following equations for all the (n-1) lines except in the lower end columns;

$$N_{1,1} \cdot \sin\beta_{1,1} \cdot \cos\theta'_{1,1} - Tm_{1,1} \cdot \cos\alpha_{1,1} \cdot \cos\theta + Hx_{1,1} - Hx_{1,2} = 0$$

$$N_{i,j} \cdot \sin\beta_{i,j} \cdot \cos\theta'_{i,j} - Tm_{i,j} \cdot \cos\alpha_{i,j} \cdot \cos\theta + Hx_{i,j} - Hx_{i,j+1} = 0$$

$$N_{n-1,m-1} \cdot \sin\beta_{n-1,m-1} \cdot \cos\theta'_{n-1,m-1} - Tm_{n-1,m-1} \cdot \cos\alpha_{n-1,m-1} \cdot \cos\theta + Hx_{n-1,m-1} - Hx_{n-1,m} = 0 \tag{8}$$

The sum of the forces in Eq. (8) is shown by

$$\sum_{i=1}^{n-1}\sum_{j=1}^{m-1} N_{i,j} \cdot \sin\beta_{i,j} \cdot \cos\theta'_{i,j} - \sum_{i=1}^{n-1}\sum_{j=1}^{m-1} Tm_{i,j} \cdot \cos\alpha_{i,j} \cdot \cos\theta + \sum_{i=1}^{n-1} Hx_{i,1} - \sum_{i=1}^{n-1} Hx_{i,m} = 0 \tag{9}$$

The resultant forces of Hx, except for the lower end columns are given by the following equation on the assumption of $Hx_{i,1}=0$ ($i=1$, n-1) (i.e., the force acting on the upper end column is assumed to be zero) and are expressed as in Fig. 5 (in this case, $m=4$ and $n=3$).

$$\sum_{i=1}^{n-1} Hx_{i,m} = \sum_{i=1}^{n-1}\sum_{j=1}^{m-1} N_{i,j} \cdot \sin\beta_{i,j} \cdot \cos\theta'_{i,j} - \sum_{i=1}^{n-1}\sum_{j=1}^{m-1} Tm_{i,j} \cdot \cos\alpha_{i,j} \cdot \cos\theta \tag{10}$$

The resultant forces of Hy in the Y axis direction can be calculated by the same

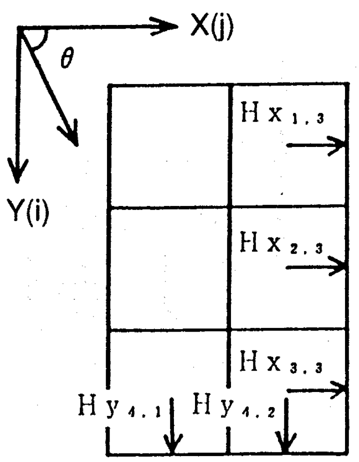

Fig. 5. Resultant sliding forces H_X and H_Y

method;

$$\sum_{j=1}^{m-1} Hy_{n,j}=\sum_{i=1}^{n-1}\sum_{j=1}^{m-1} N_{i,j}\cdot\sin\beta_{i,j}\cdot\sin\theta'_{i,j}-\sum_{i=1}^{n-1}\sum_{j=1}^{m-1} Tm_{i,j}\cdot\cos\alpha_{i,j}\cdot\sin\theta \tag{11}$$

The following equation is established with Eqs. (10) and (11) taking into account the equilibrium of the forces that are the right angle components of Hx and Hy to the sliding direction of the assumed sliding mass, except for the lower end columns.

$$\sum_{i=1}^{n-1} Hx_{i,m}\cdot\sin\theta-\sum_{j=1}^{m-1} Hy_{n,j}\cdot\cos\theta=0 \tag{12}$$

The sliding direction is calculated using Eqs. (10), (11) and (12).

$$\tan\theta=\frac{\sin\theta}{\cos\theta}=\sum_{j=1}^{m-1} Hy_{n,j}\Bigg/\sum_{i=1}^{n-1} Hx_{i,m}$$

$$=\frac{\sum_{i=1}^{n-1}\sum_{j=1}^{m-1} N_{i,j}\cdot\sin\beta_{i,j}\cdot\sin\theta'_{i,j}-\sum_{i=1}^{n-1}\sum_{j=1}^{m-1} Tm_{i,j}\cdot\cos\alpha_{i,j}\cdot\sin\theta}{\sum_{i=1}^{n-1}\sum_{j=1}^{m-1} N_{i,j}\cdot\sin\beta_{i,j}\cdot\cos\theta'_{i,j}-\sum_{i=1}^{n-1}\sum_{j=1}^{m-1} Tm_{i,j}\cdot\cos\alpha_{i,j}\cdot\cos\theta} \tag{13}$$

There are three parameters, $N_{i,j}$, θ and $\alpha_{i,j}$, on the right side of Eqs. (10) and (11). The angle $\alpha_{i,j}$ is the function of θ as seen in Eq. (5). The resultant forces in Eqs. (10) and (11) therefore must be calculated by iterative procedures as follows: $\alpha_{i,j}$, $N_{i,j}$ and $Tm_{i,j}$ first are calculated using Eqs. (5), (4) and (3), assuming the angle of θ. Eq. (12) then can be examined.If Eq. (12) is not satisfied, a different angle for θ is assumed, and Eq. (12) again examined. As this equation generally is not satisfied strictly, the following inequality is checked;

$$\left|\sum_{i=1}^{n-1} Hx_{i,m}\cdot\sin\theta-\sum_{j=1}^{m-1} Hy_{n,j}\cdot\cos\theta\right|\leq\delta \tag{14}$$

If this inequality is not satisfied, calculations using Eqs. (5), (4) and (3) are made again for another assumed sliding direction. If Eq. (14) is satisfied, the sliding direction of the assumed sliding mass is considered to be that direction.

In the report, δ in Eq. (14) was assumed to be 0.98 kN, the increment or decrement in θ being set at 0.005 radian. δ was set to satisfy Eq. (14) when θ was changed at every 0.005 radian under the mean dimension of a column $10\times 10\times 1$m. The angle calculated using the following equation was adapted as the initial assumed value for θ.

$$\tan\theta=\sum_{i=1}^{n-1}\sum_{j=1}^{m-1}(\sin\theta'_{i,j}/\cos\theta'_{i,j}) \tag{15}$$

(3) Setting up the resisting surface in the lower end column

The lower end columns are regarded as the soil mass that resists the sliding force caused by the upper sliding column of the assumed sliding mass. The horizontal surface on which the resisting force acts was set in the respective lower end columns. The resisting surface of the assumed sliding surface therefore was considered to be composed of many horizontal surfaces, although the actual resisting surface had the general appearance of a curved continuous plane. The

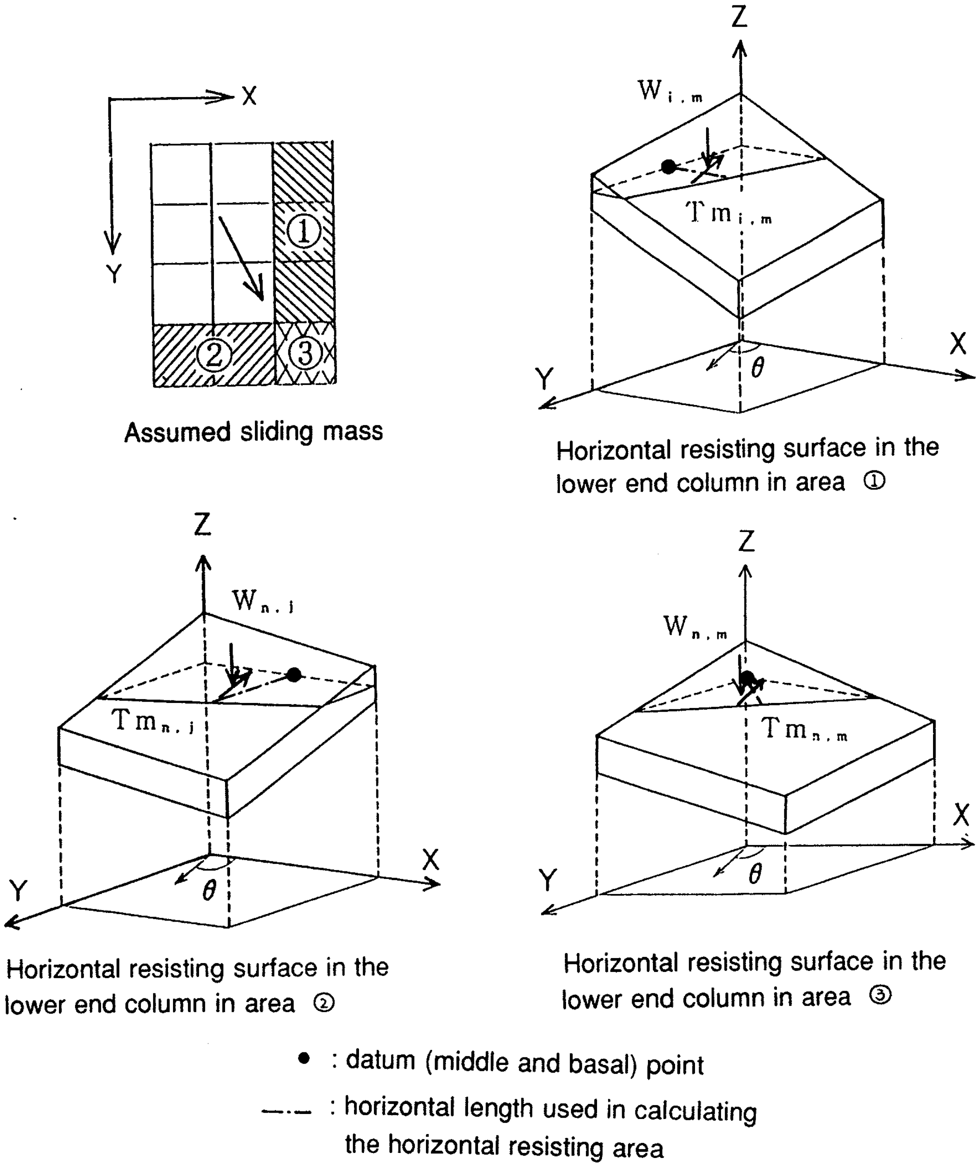

Fig. 6. Setting the horizontal resisting plane in the lower end columns

horizontal resisting surface was set in the lower end columns as follows (see, Fig. 6): 1) For the right and lower sides of the assumed sliding mass (areas ① and ② in Fig. 6), the horizontal plane was set at every column through the middle and basal point on an imaginary vertical wall between the sliding and resisting (lower end) columns. 2) For the corner column (area ③ in Fig. 6), the plane was set through the base point of the left and upper grid point of the resisting column.

The mobilized resisting shear forces of $Tm_{i,j}$ acting on these resisting surfaces were expressed as follows:

In the lower end column in area ①

$$Tm_{i,m}=\frac{c\cdot A_{i,m}+W_{i,m}\cdot\tan\phi}{F}\qquad(i=1,\cdots,n-1)\tag{16}$$

In the lower end column in area ②

$$Tm_{n,j}=\frac{c\cdot A_{n,j}+W_{n,j}\cdot\tan\phi}{F}\qquad (j=1,\cdots,m-1)\tag{17}$$

In the lower end column in area ③

$$Tm_{n,m}=\frac{c\cdot A_{n,m}+W_{n,m}\cdot\tan\phi}{F}\tag{18}$$

The area of the horizontal surface was calculated by multiplying the mesh space by the horizontal length between the middle and basal point. The slope surface point that was obtained by setting a horizontal line along the sliding direction. But, if the inclination of the slope surface is very gentle, the horizontal length becomes too long. The resisting surface is abnormal as compared to that of the actual failed slope. In such a case, $Tm_{i,j}$ was calculated as $W_{i,j}=W_{i,j}/2$, and $A_{i,j}=(D)^2$ (in which, D is the mesh space) in Eqs. (16), (17) and (18).

(4) Calculation of the safety factor

The safety factor was calculated on the basis of the equilibrium of the forces acting on the assumed sliding mass. These forces are shown in Fig. 7. The sliding force (H) acting on an imaginary vertical wall between the assumed sliding and lower end columns, obtained from Eqs. (10) and (11), is expressed by

$$H=\sum_{i=1}^{n-1}Hx_{i,m}\cdot\cos\theta+\sum_{j=1}^{m-1}Hy_{n,j}\cdot\sin\theta\tag{19}$$

The total resisting force acting on the lower end column is

$$T=\sum_{i=1}^{n-1}Tm_{i,m}+\sum_{j=1}^{m-1}Tm_{n,j}+Tm_{n,m}\tag{20}$$

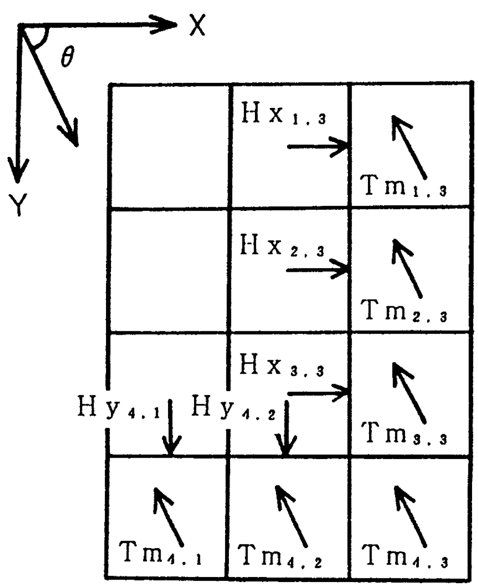

Fig. 7. Resultant forces acting on an imaginary vertical wall between the assumed sliding columns and the lower end columns

The inequality then is checked;

$$|H-T| \leq \varepsilon \tag{21}$$

If this inequality is not satisfied, calculations using Eq. (4) are made again with another assumed safety factor. If Eq. (21) is satisfied, the safety factor of the assumed sliding mass is assumed to be that safety factor. In the numerical calculations, the initial safety value was assumed to be 2.00. The increment or decrement in this safety factor was set at 0.01, and the allowable error, ε, for the iterative procedure in Eq. (21) at 5.9 kN. The value was set to satisfy Eq. (21) when the safety factor was changed every 0.01 increment for the mean dimension of a column $10 \times 10 \times 1$m.

(5) Determination of the most critical sliding direction

An analysis area composed of 7×7 columns was set. A sliding mass was assumed such that all combinations of columns were set in the analysis area. The sliding direction and safety factor were obtained for each assumed sliding mass as described earlier. The most critical sliding mass is regarded to be the one that has the minimum safety factor value.

3. APPLICATION TO FAILED SLOPES

3.1 *Outline of the test field*

This method was applied to actual failed slopes in the Irisugaya test field. The test field,

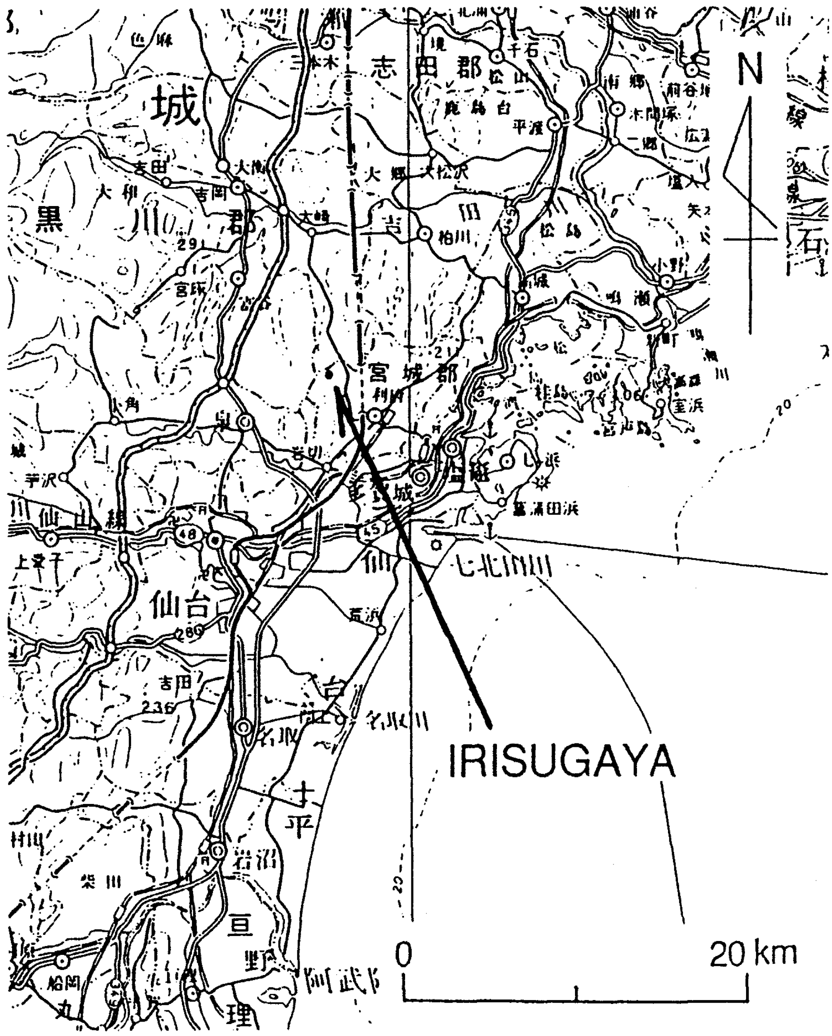

Fig. 8. Site map of the Irisugaya test field (Rifu-cho, Miyagi Prefecture, Japan)

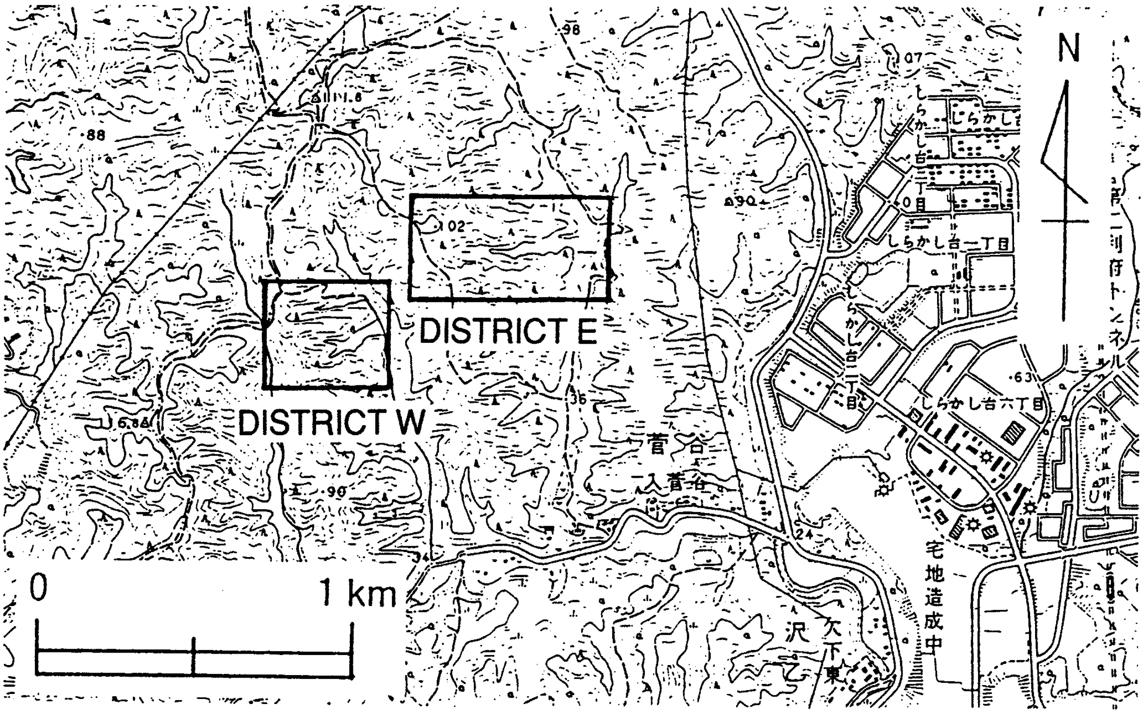

Fig. 9. Topographical map of the Irisugaya test field (District W is the test field in this study)

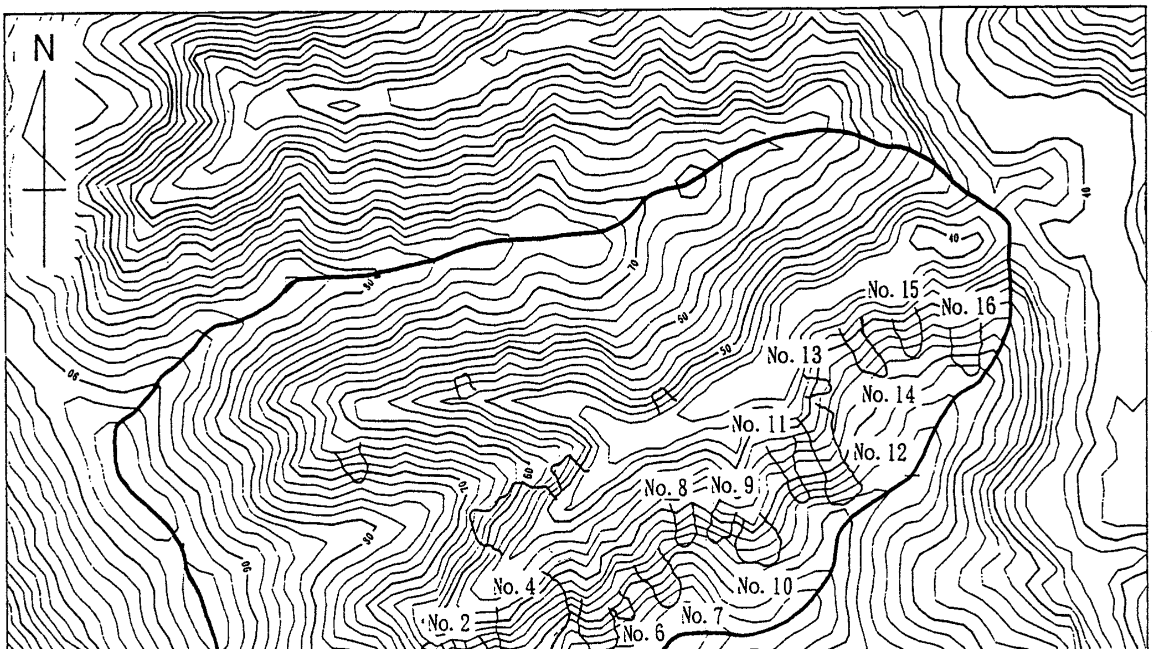

Fig. 10. Topographical map of district W in the Irisugaya test field (1986 failures)

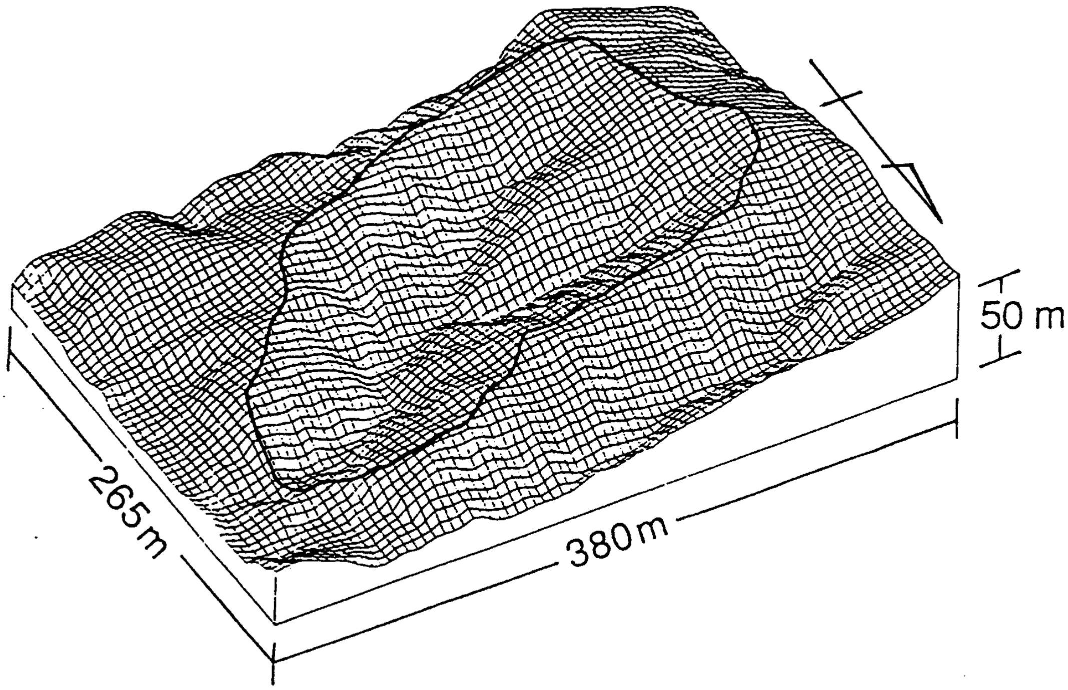

Fig. 11. Block diagram of district W in the Irisugaya test field

composed of the alternating layers of sand and silt stone mixed with tuff, is in Rifu-cho, Miyagi Prefecture, Japan [11] and covers about 22 hectares. Fig. 8 shows the site map of the test field and Fig. 9 the topographic map of this district. A forest fire occurred in the test field on 27 April 1983, and many mountain slope failures caused by heavy rainfall took place in the district on 5 August 1986. The W district shown in Fig. 9 is the test field used in this study.

Aerial photographs that covered the test field were taken by the Geographical Survey Institute, Ministry of Construction in November 1984 (scale, 1/10,000) and in August 1986 (scale 1/6,000), and digital land elevation models of the slope (mesh space, 5 m) were constructed using these photographs. Fig. 10 shows the topographic map of the test field drawn from data obtained from the digital elevation model shown in Fig. 11. The sites and shapes of the failures that occurred in 1986 are shown in Fig. 10.

3.2 *Predicted results for the unstable cell*

The unstable cell for the test field shown in Fig. 10 was calculated using the prediction method [4]. The depth of the potential failure layer must be input to the model. The mean (1.15 m) of the depths measured was regarded to be the depth of the potential failure layer at each grid point in the predicting method because depth investigation at every grid point is impossible in a large test field. The soil input data shown in Table 1 were obtained on the actual slope or in the laboratory. The effective rainfall intensity used was 30 mm/h, continuing for 30 hours. The degree of instability for potential failure was defined in terms of the safety factor as the continuous period (t_{cr}) until the safety factor becomes less than unity. The degree of instability was classified as

A: $0 < t_{cr} \leqq 5$ hours   B: $5 < t_{cr} \leqq 10$ hours
C: $10 < t_{cr} \leqq 15$ hours   D: $15 < t_{cr} \leqq 20$ hours
E: $20 < t_{cr} \leqq 25$ hours   F: $25 < t_{cr} \leqq 30$ hours

Results are shown in Fig. 12. The unstable cells (classes A and B) appeared at or within the failed site.

Table 1. Soil input data

γ_t (tf/m^3)	γ_{sat} (tf/m^3)	tan ϕ'	c' (tf/m^2)
1.73	1.80	0.75 (ϕ'=37°)	0.28

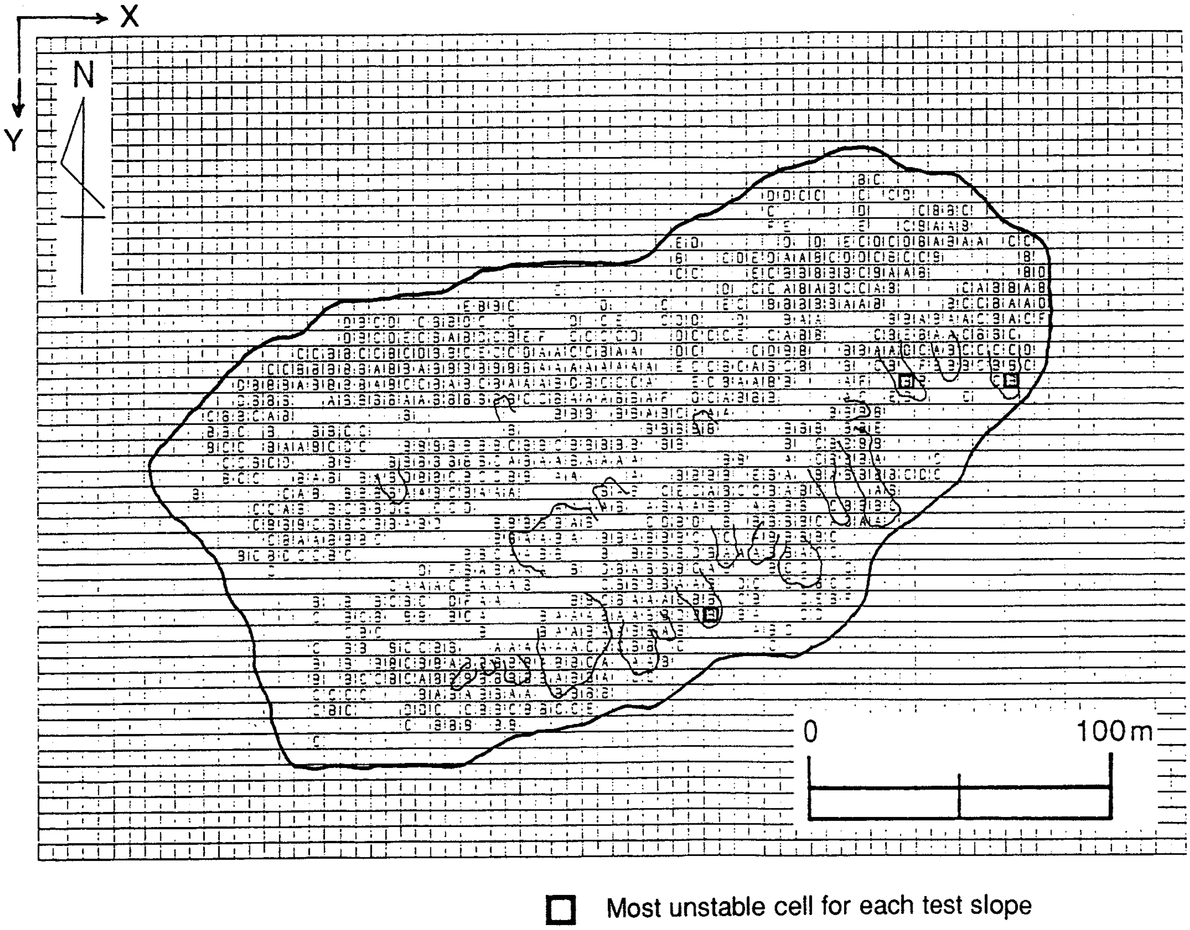

Fig. 12. Unstable cells

3.3 *Results calculated for the sliding direction*

(1) Test slopes

Three slopes (Nos. 7, 14, and 16, see Fig. 10) were selected for testing from the 16 slopes that failed in 1986. Field investigations used a simplified penetration test to ascertain the depth of the surface layer. These slopes were selected because the scars caused by their failures had simple shapes, not the complicated ones caused by more than two failures.

The area of analysis was set using 7×7 columns, the most unstable cell appearing at the center. In the test field, the most unstable cells (classes A and B) were calculated, and these appeared at the actual failed slopes as shown in Fig. 12. The most unstable cell therefore was defined as the unstable cell that appeared at the upper end of the valley. The most unstable cells by this definition are the squares enclosed by a thick line in Fig. 12.

Three digital elevation models were constructed on the basis of the data obtained from the aerial photographs taken in 1986. The slope surface elevation at the failed site was estimated by referring to the longitudinal and transverse planes. The depths of the potential failure layers were

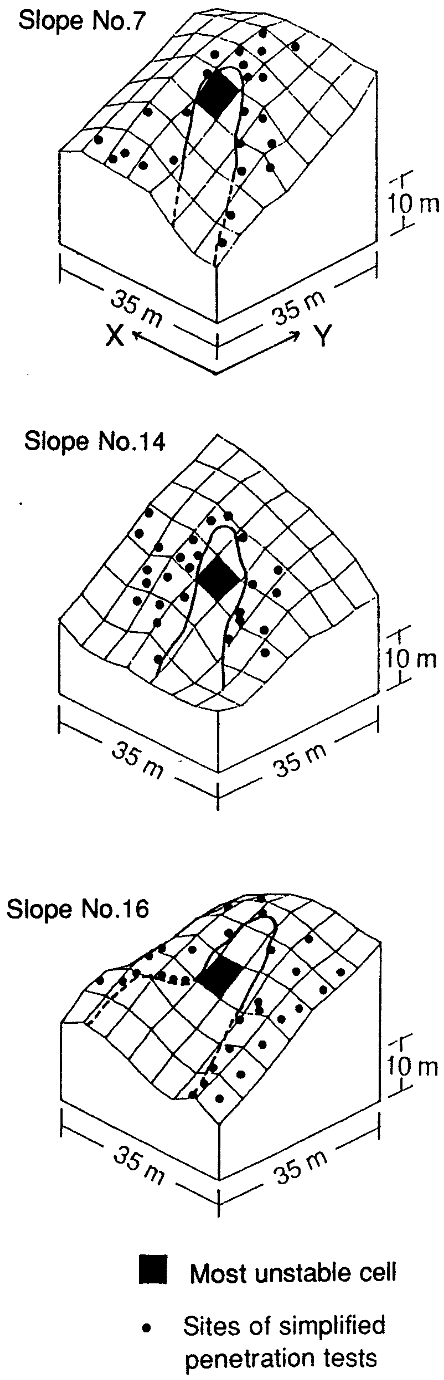

Fig. 13. Block diagrams of the three test slopes

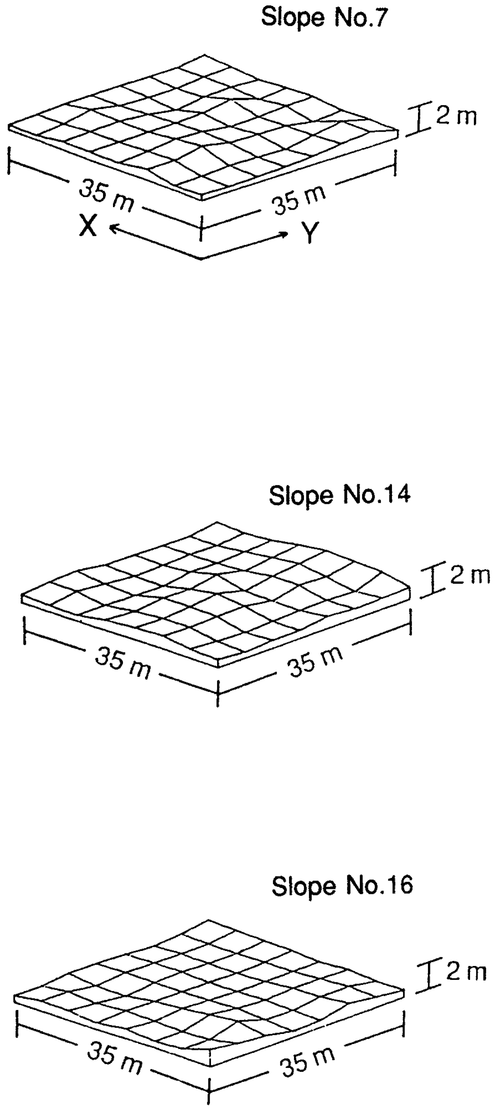

Fig. 14. Depths of the potential failure layers on the test slopes

assessed by simplified penetration tests in 1990, 1991 and 1992. Thus depth was defined as $N_{10}=10$ (meaning that ten times a 49 N weight must be dropped from a height of 50 cm to penetrate 10 cm). The depth at the grid points was interpolated on the basis of the site and the measured depth[12]. Block diagrams of the test slopes are shown in Fig. 13, and the depths of the potential failure layer in Fig. 14. The curved lines in Fig. 13 delineated the forms of the actual failed masses, dotted lines denuded or eroded shapes. The points indicate the sites at which the depth of the potential feilure layer was measured.

(2) Results calculated for the sliding direction

The calculation method proposed in section 2 was used for slopes 7, 14 and 16. Fig. 15 shows the failed shapes, the arrows indicating the calculated direction of the critical sliding mass. Although the actual failed sliding directions for slopes 7 and 14 differed markedly from the

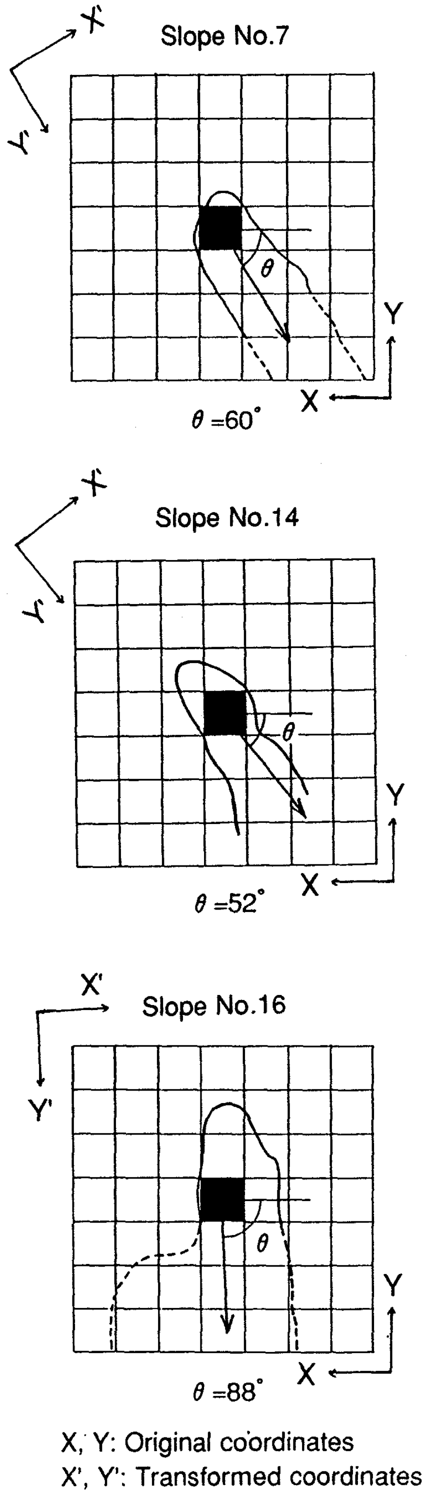

Fig. 15. Calculated sliding directions

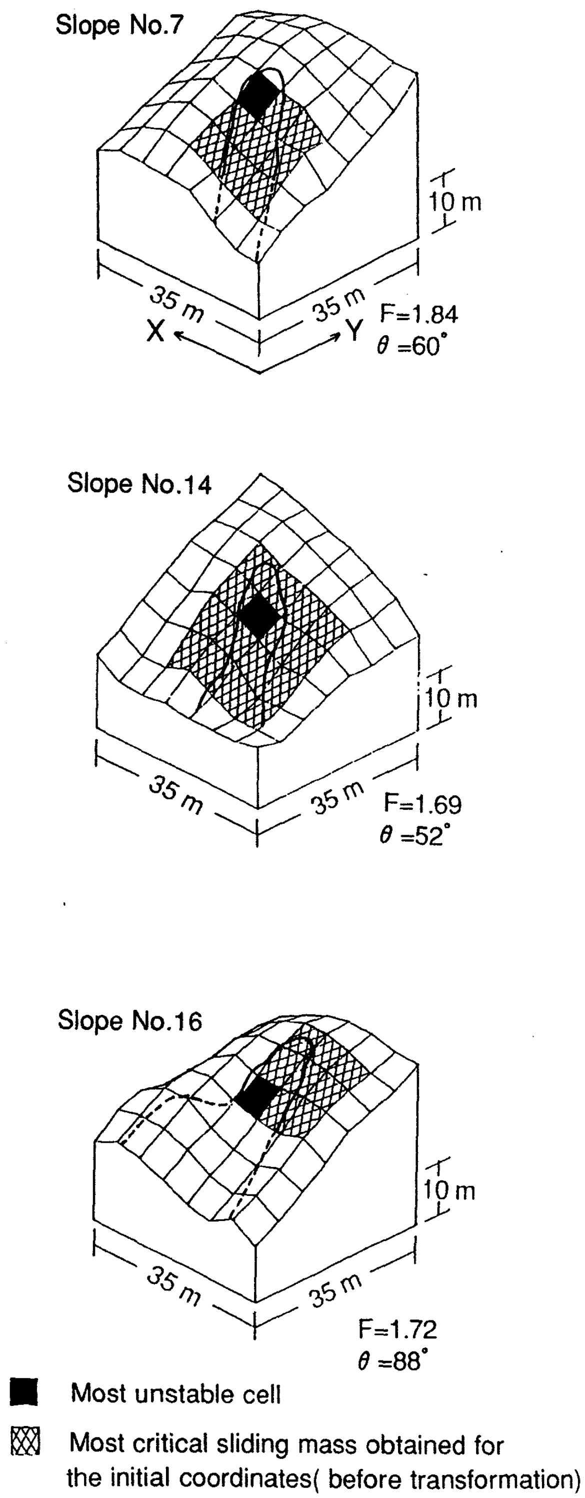

Fig. 16. Most critical sliding mass obtained for the initial coordinates

direction of the Y axis, the sliding direction obtained is nearly equal to that of the actual failed mass. Good results also were obtained for slope No.16, the actual sliding direction of the slope not differing greatly from the direction of the Y axis. The proposed method therefore is considered appropriate for calculating the probable direction of a shallow failure.

3.4 *Results calculated for the most critical sliding mass*

The most critical sliding mass obtained for the sliding direction was determined (Fig. 16). The shapes obtained were very different from those of the actual failed mass. In predicting the shape of the most unstable sliding mass, we therefore can not use the results obtained by the proposed method.

To predict the shape of a probable failure more reliably, the sliding direction calculated by the proposed method can be used as the probable direction, but the probable failure shape must be predicted by another method in which the direction is defined as the steepest direction of the most unstable cell. The coordinates then are transformed so that the new Y axis (Y′) is parallel to the direction obtained because the force equilibrium in the 3-D MPSS method was analyzed along both the steepest and cross-sectional direction [5].

3.5 *Probable failure shape results*

The coordinates were transformed by a method that produces grid points from randomly distributed data [12], grid point data (height of the slope surface) before transformation being assumed to be random. Transformed data were obtained on the assumption that the original point transformed is at the center of the most unstable cell. The analysis area within which the most critical sliding mass was identified then was established so as to include seven columns in the longitudinal and the transverse directions. Many assumed sliding masses that were regarded to be rectangular in plan shape were set up within the area. The method of setting an assumed sliding mass as non-rectangular [7] was applied to the assumed sliding mass (rectangular). The non-failure column had been defined by taking into account the continuity of the internal forces acting on an imaginary vertical wall between columns [7]. The most critical, unstable sliding mass was calculated by 3-D slope stability analyses using the MPSS method, and the Hovland and simplified Janbu methods.

(1) 3-D MPSS method results for a rectangular sliding shape

Fig. 17 shows the most critical unstable masses obtained using the 3-D MPSS method combined with a rectangular sliding shape. The shaded areas in Fig. 17(a) show the most critical unstable masses for the sliding direction calculated. For slope 7 the result appears to be nearly as the long as and within the failed site. For slope 14 the result was nearly equal to the failed mass in terms of both the length and site. The right side of the critical unstable mass facing down slope, however, could not be predicted as the critical area. The most critical unstable mass for slope 16 covered the actual failed mass, but in places the shape obtained is larger than the actual failed shape, especially at the left upper end of the column. Setting the shape of an assumed sliding mass as non-rectangular therefore was required for better prediction. Subsequent calculations were made for a non-rectangular sliding shape.

The shaded areas in Fig. 17(b) show the most critical unstable mass calculated on the assumption that the sliding direction is the same as the steepest direction of the most unstable cell (This assumption was used in previous reports [5, 6 and 7]). The same results were obtained for slopes 7 and 14, but the length was too long for slope 16.

(2) 3-D MPSS method results for a non-rectangular sliding shape

Fig. 18 shows the most critical unstable masses obtained using the 3-D MPSS method combined

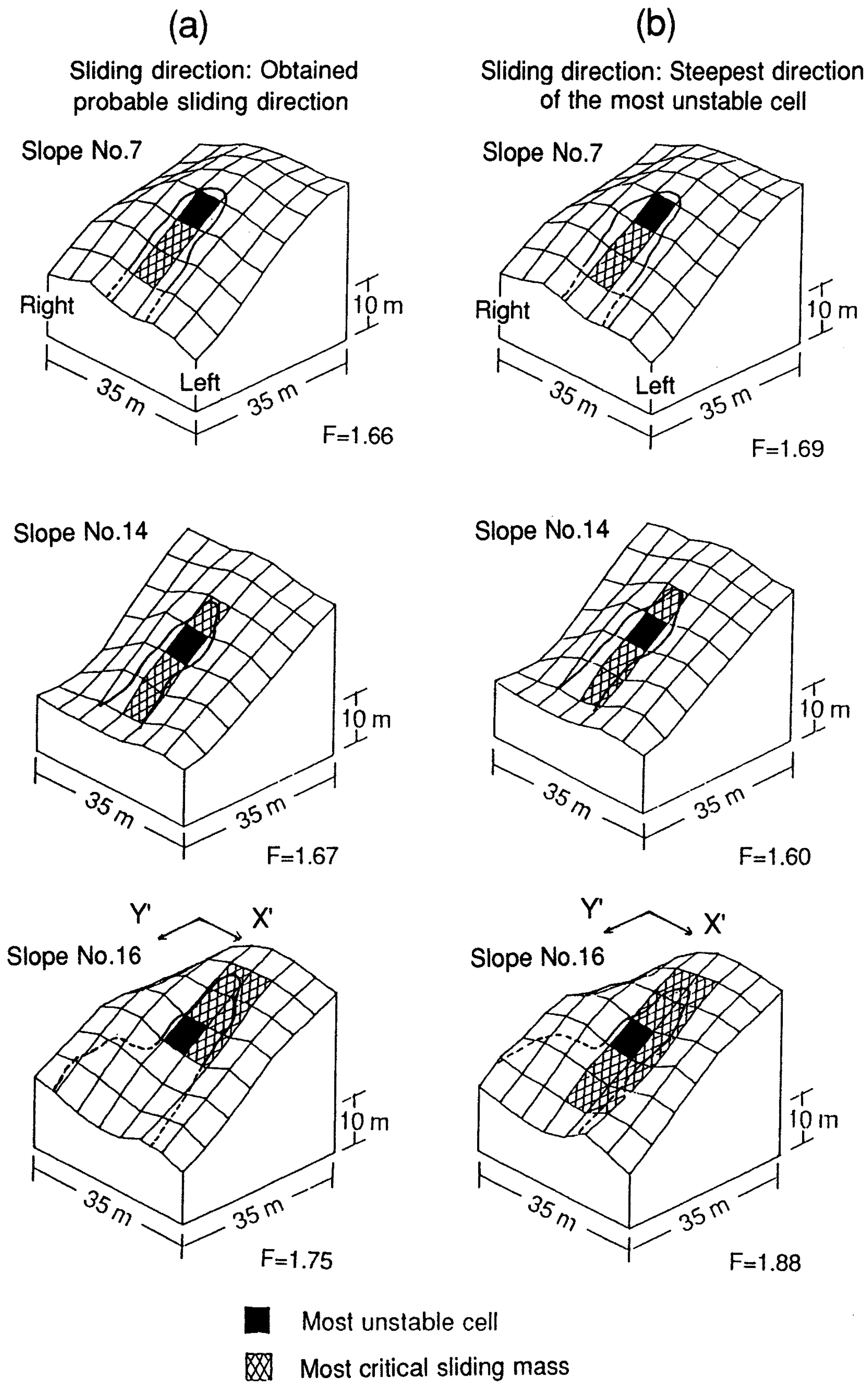

Fig. 17. Simulation results obtained by the 3-D MPSS method for a sliding mass rectangular in shape

with a non-rectangular assumed sliding mass. Fig. 18(a) shows the results calculated using the probable sliding direction obtained by our proposed method. Results for slope 7 were equivalent to the results obtained for a rectangular shape (see Fig. 17(a)). For slopes 14 and 16, the results were better than those shown in Fig. 17(a).

Fig. 18(b) shows the results calculated by setting the Y' axis to be the same as the steepest direction of the most critical unstable cell. The result for slope 7 was the same as that for the

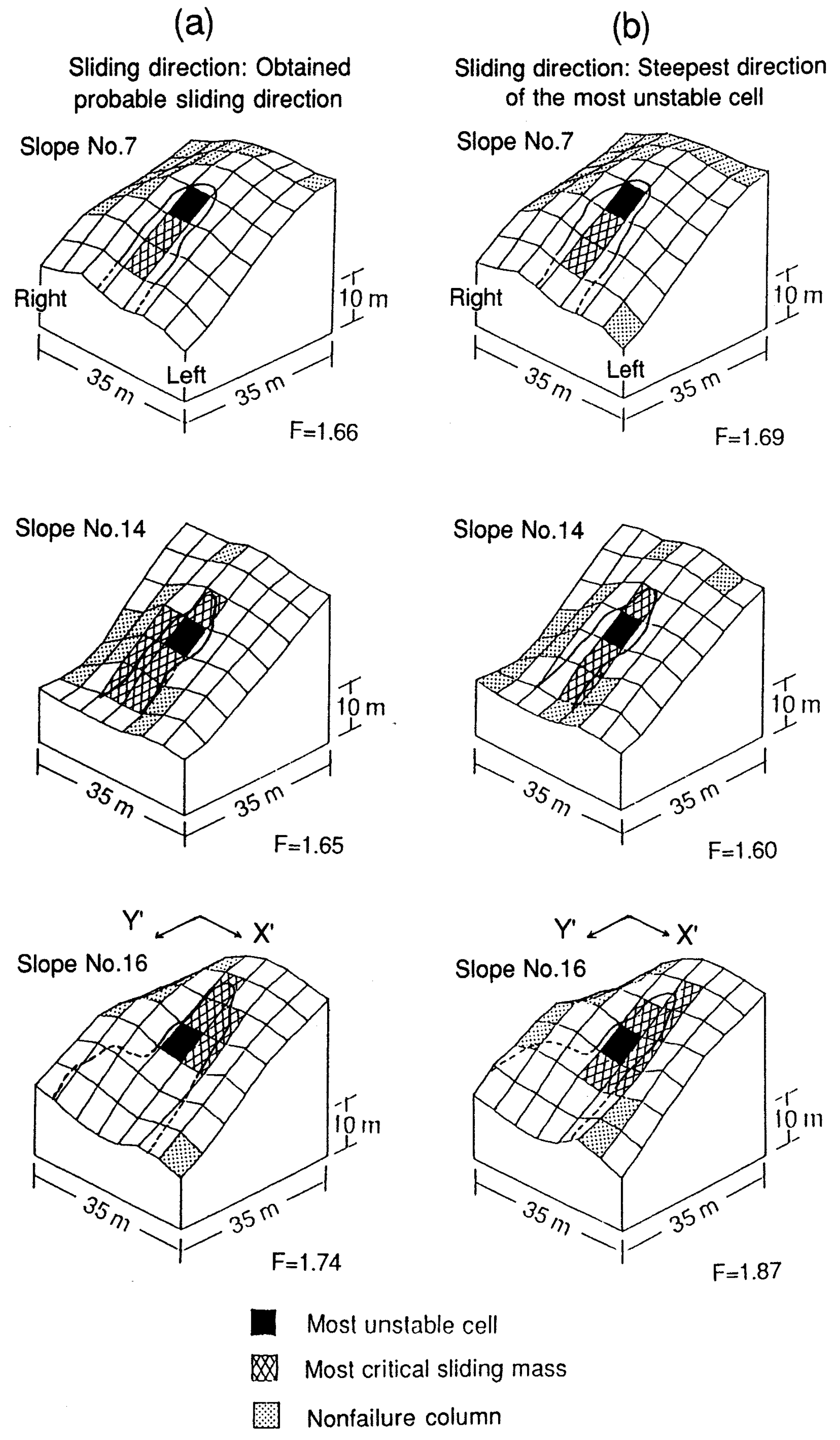

Fig. 18. Simulation results obtained by the 3-D MPSS method for a sliding mass non-rectangular in shape

calculated sliding direction. For slope 14, the result differed somewhat from that obtained using the calculated direction, but was the same as for the rectangular assumed sliding mass (see Fig. 17(b)). For slope 16, results showed that it differed in places from the shape of the actual failed mass

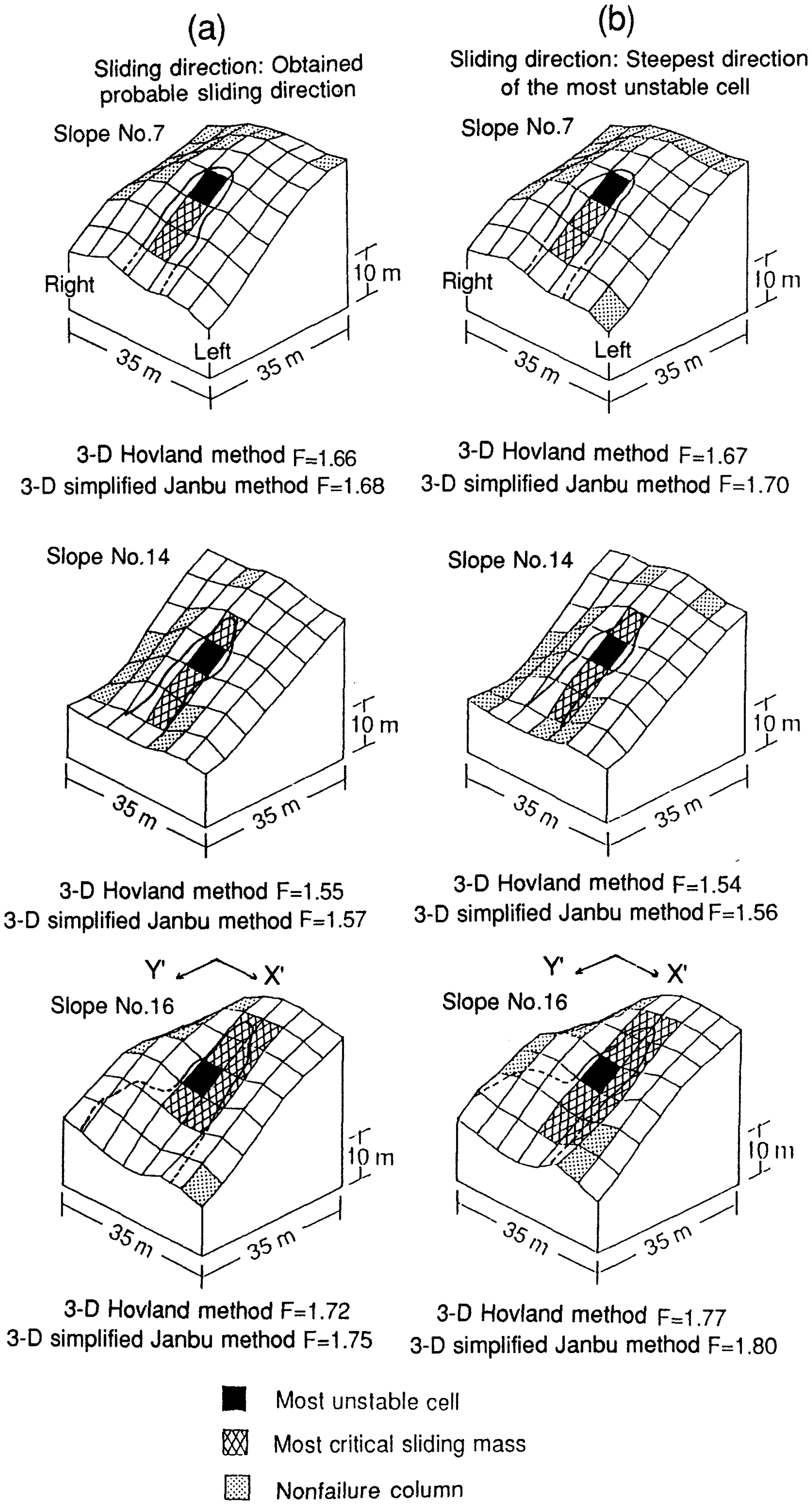

Fig. 19. Simulation results obtained by the 3-D Hovland and 3-D simplified Janbu methods for a sliding mass non-rectangular in shapes

(3) Results using the Hovland and simplified Janbu methods for a non-rectangular sliding shape

Fig. 19 shows the most critical unstable sliding masses obtained using the 3-D Hovland and simplified Janbu methods combined with a non-rectangular shape. Results for the sliding direction calculated are shown in Fig.19(a). These show that the shapes obtained are the same for the Hovland method as for the simplified Janbu method, and that the shape of the critical unstable sliding masses is rectangular in spite of the assumption of a non-rectangular shape. Results for slopes 7 and 14 are the same as those obtained using the 3-D MPSS method with the rectangular shape. For slope 16, the result gives somewhat too long a length.

Fig. 19(b) shows the results calculated for the direction of the steepest direction of the most unstable cell. The shapes obtained also were the same for the two methods, appearing as rectangular. The results for slopes 7 and 14 were the same as in Fig. 19(a). For slope 16, the result appeared to be too long.

Better results therefore can be obtained by the calculating the sliding direction as proposed here.

3.6 *Comparison of the results for different sliding directions and the 3-D analyses*

Two parameters proposed elsewhere [13] were used to determine which results are better for the prediction of the site and shape of the most probable failure. These are defined by the equations;

$$\text{Proved Percent}(\%) = (M / Nm) \times 100 \tag{22}$$

$$\text{Represented Percent}(\%) = ((N_t - N_m - N_0 + 2M) / N_t) \times 100 \tag{23}$$

in which, N_t is the total number of columns in the analysis area (in the study, $N_t=49$), N_m the number of columns in the critical unstable mass, N_0 the number of columns in the actual failed mass, and M the number of columns that coincides with the predicted and actual failed columns.

The calculated results are shown in Table 2 Results for the assumption of the sliding direction

Table 2. Proved and represented percentages for the four types of 3-D slope stability analyses

		rectangular	non-rectangular		
		MPSS	MPSS	Hovland	simplified Janbu
	Slope No.7	100 (100)	100 (100)	100 (100)	100 (100)
	Slope No.14	100 (100)	100 (100)	100 (100)	100 (100)
	Slope No.16	83 (60)	100 (71)	63 (60)	63 (60)
	Slope No.7	86 (86)	86 (86)	86 (86)	86 (86)
	Slope No.14	92 (92)	98 (92)	92 (92)	92 (92)
	Slope No.16	98 (92)	100 (94)	94 (92)	94 (92)

MPSS: multi-planar sliding surface method
( ) results obtained on the assumption that the sliding direction is that of the most unstable cell

is being the same as that for the most unstable cell are shown in parentheses. The results calculated for the non-rectangular shape are better than those for the rectangular shape, as has also been reported elsewhere [7]. Each value of the two parameters for the calculated sliding direction is equal to, or larger than, the value for the cell's steepest direction. The proposed method therefore is shown to be an appropriate one. Of the three slope stability analysis methods combined with a non-rectangular shape, results calculated using the 3-D MPSS method are better for the prediction of the site and shape of a probable unstable failure than are those calculated by the other slope stability analysis methods.

4. CONCLUSIONS

1) A method by which to calculate the sliding direction of an assumed sliding mass was proposed on the assumption that internal forces are balanced at a right angle to the sliding direction.
2) Results obtained by application to actual failed slopes showed that the sliding direction calculated was very close to that of the actual failed mass. The shape of the most unstable mass, however, differed markedly from that of the failed mass.
3) The sliding direction obtained using the proposed method was used to transform the coordinates of a digital land elevation model, and slope stability was analyzed using three 3-D methods: the multi-planar sliding surface method, and the 3-D Hovland and simplified Janbu methods. The values of the two parameters used in the study showed that the results calculated using the proposed sliding direction were better for the prediction of probable unstable failure than were those obtained using the most unstable cell's sliding direction.
4) Results for the 3-D multi-planar sliding surface method were more appropriate than those obtained by the other analysis methods.

The safety factors shown in Figs. 17, 18 and 19 are greater than unity because the groundwater movement model, which had been used to obtain the most unstable cell, was not used in the 3-D calculations. More reliable predictions can be made by incorporating the root resistance of vegetation into the 3-D methods. In a failure study, a debris flow caused by a mountain slope failure will be simulated that is based on the probable unstable soil volume calculated using 3-D slope stability analysis methods.

ACKNOWLEDGEMENTS

I am deeply grateful to Professor Masaru Nishi of Kobe University and Associate Professor Kenji Kashiwaya of Kanazawa University for their expert guidance, and to Mr. Tsutomu Maeda, Mr. Yohei Suzuki, and Mr. Katsuhiko Morimoto, former graduate students of Kobe University, for their assistance with the calculations.

Part of this research was supported by Grants-in-Aid for Scientific Research received in 1990, 1991 and 1992 (02201121, 03201129 and 04201126: Principal investigator, Professor Tamotsu Takahashi, Kyoto University) from the Ministry of Education, Science and Culture Japan.

References

[1] Yagi, N., Yatabe, R. and Enoki, M. (1985)., Laboratory and field experiments on prediction method of occurring time of slope failure due to rainfall, *Journal of the Japan Landslide Society*, 22–2, pp.1–7 (in Japanese with English abstract).

[2] Hiramatsu, S., Mizuyama, T. and Ishikawa, Y. (1990)., Experimental study on characteristics of vertical unsaturated seepage, *Journal of the Japan Society of Erosion Control Engineering*, 43–2, pp.3–10 (in

Japanese with English abstract).
[3] Okimura, T. (1983)., A slope stability method for predicting rapid mass movements on granite mountain slopes, *Journal of Natural Disaster Science*, 5–1, pp.13–30.
[4] Okimura, T. and Ichikawa, R. (1985)., A prediction method for surface failures by movements of infiltrated water in a surface soil layer, *Journal of Natural Disaster Science*, 7–1, pp.41–51.
[5] Okimura, T. and Maeda, T. (1990)., A three-dimensional multi-planar sliding surface method to predict an area of surface failure, *Journal of the Japan Society of Erosion Control Engineering*, 44–4, pp.3–10 (in Japanese with English abstract).
[6] Okimura, T. and Morimoto, K. (1992)., Some examinations of the application of the 3-D multi-planar sliding surface method, *Journal of the Japan Society of Erosion Control Engineering*, 45–3, pp.13–17 (in Japanese).
[7] Okimura, T. (1993)., Comparison of shapes of a shallow failure by shaping forms of an assumed sliding mass and different slope stability analyses, *Proceedings of the Third ROC and Japan Joint Seminar on Natural Hazard Mitigation*, pp.490–504
[8] Hovland, H.J. (1977)., Three-dimensional slope stability analysis, Proc. ASCE, 103-GT9, pp.971–986.
[9] Ugai, K. (1987)., Three-dimensional slope stability analysis by simplified Janbu method, *Journal of the Japan Landslide Society*, 24–3, pp.8–14 (in Japanese with English abstract).
[10] Okimura, T. and Tanaka, S. (1980)., Researches on soil horizon of weathered granite mountain slope and failed surface depth in a test field, *Journal of the Japan Society of Erosion Control Engineering*, 33–1, pp.7–16 (in Japanese with English abstract).
[11] Oide, K., Nakagawa, H. and Kanisawa, S. (1980)., Geology in Japan (2), Tohoku District, Kyoritsu-Shuppan, Tokyo, pp.7–16 (in Japanese).
[12] Ozaki, E., Okimura, T. and Kashiwaya, K. (1991)., Construction of a simple landform surveying system, *Memoirs of the Graduate School of Science and Technology of Kobe University*, 9-B, pp.23–40 (in Japanese with English abstract).
[13] Michiue, M., Fujita, M. and Hosotani, M. (1988)., Prediction of mountain slope failure, *Memoirs of the Faculty of Engineering of Tottori University*, 19–1, pp.71–82 (in Japanese with English abstract).
[14] Okimura, T., Maeda, T. and Suzuki, Y. (1990)., An examination of the three-dimensional multi-planar sliding surface method, *Bulletin of Reclamation Engineering Research Institute, Faculty of Engineering of Kobe University*, 9, pp.67–101 (in Japanese).